A predictive interatomic potential for He in Cu and Nb

2011 Modelling Simul. Mater. Sci. Eng. 19 035007

(http://iopscience.iop.org/0965-0393/19/3/035007)

Modelling Simul. Mater. Sci. Eng. **19** (2011) 035007 (8pp) doi:10.1088/0965-0393/19/3/035007

A predictive interatomic potential for He in Cu and Nb

A Kashinath[1] **and M J Demkowicz**

Department of Materials Science and Engineering, Massachusetts Institute of Technology, 77 Massachusetts Avenue, Cambridge, MA 02139, USA

E-mail: abishekk@mit.edu and demkowicz@mit.edu

Received 18 October 2010, in final form 14 February 2011
Published 16 March 2011
Online at stacks.iop.org/MSMSE/19/035007

Abstract
First principles calculations show that two-body forces are sufficient to describe interactions of He with fcc Cu and bcc Nb. This property is explained directly from calculated charge density distributions and used to construct a Cu–Nb–He interatomic potential that predicts accurate He impurity energies despite not being fitted to them.

(Some figures in this article are in colour only in the electronic version)

1. Introduction

He produced by (n, α) transmutation reactions plays an important role in the microstructural evolution of irradiated materials [1]. In crystalline solids, He leads to bubble formation [2] and growth into voids [3], blistering [4], as well as accelerated swelling [5] and embrittlement [6]. He-implanted Cu–Nb multilayer nanocomposites, however, have shown reduced He-induced degradation compared with pure Cu or Nb [7–9]. Insight into the behavior of He in Cu–Nb multilayers may be obtained using atomistic simulations, but a reliable Cu–Nb–He potential is required. Here we describe the construction of such a potential.

Previous efforts to construct Cu–He [10] and Nb–He [11] potentials were based on the Hartree–Fock–Slater approximation and a numerical integration scheme developed by Wedepohl [12]. We use density functional theory (DFT) calculations to show that He interacts with fcc Cu, bcc Nb and other He atoms in fcc Cu and bcc Nb through short-range, radial, environment-independent forces. These forces are used to obtain two-body interaction potentials for He in Cu and Nb that predict He impurity formation energies in excellent agreement with DFT.

2. Methodology

DFT calculations are carried out under periodic boundary conditions using the Quantum ESPRESSO code [13]. For Cu, the Rabe–Rappe–Kaxiras–Joannnopolous ultrasoft

[1] Author to whom any correspondence should be addressed.

Table 1. Comparison between DFT-calculated and experimental values of lattice parameter (a_0), cohesive energy (E_{coh}) and bulk modulus (B) for Cu and Nb.

Quantity	a_0 (Å)	E_{coh} (eV)	B (GPa)
Cu, DFT (GGA)	3.676	3.474	139.02
Cu, DFT (LDA)	3.551	4.459	170.01
Cu, experiment	3.615 [20]	3.54 [21]	142.0 [22]
Nb, DFT (GGA)	3.310	7.293	168.0
Nb, experiment	3.3008 [23]	7.47 [24]	173.0 [22]

pseudopotential [14] and for Nb, the Vanderbilt ultrasoft pseudopotential [15] is used. For both Cu and Nb, the Perdew–Burke–Ernzerhof generalized gradient approximation (GGA) [16] exchange-correlation functional is employed. Selected results are compared with calculations carried out using the local density approximation (LDA) [17]. An energy cut-off for wavefunctions of 800 eV is chosen and Methfessel–Paxton smearing of 0.14 eV is applied to perform the Brillouin zone (BZ) integration. The BZ is sampled using a Monckhorst–Pack k-point mesh and all calculations are checked for k-point convergence. Table 1 shows that selected physical properties calculated at 0 K for fcc Cu and bcc Nb are in reasonable agreement with experimentally determined values. Consistent with previous studies, GGA overpredicts equilibrium lattice parameters and underpredicts cohesive energies. The opposite is true of LDA [18, 19].

Forces between He and other atoms X (Cu, Nb, or He) are calculated as functions of interatomic distance, r, via three methods. In the first, the force between atoms in a He–X dimer is found as a function of bond length. In the second, a He atom is inserted into a high symmetry site in a perfect crystal of X and the forces on all atoms are calculated without allowing the atomic structure to relax. Due to the symmetry of the crystal, the net force on the He atom is zero, as is the net force on any X atom due to all other X atoms. Thus, any resultant force on an X atom is due to interactions with He. Varying the lattice parameter of the crystal modifies He–X interatomic distances and allows the full force–distance curve to be computed.

The third method can be used to calculate forces due to a He atom inserted into any chosen configuration of X atoms. First, the forces F_X exerted by X atoms on each other in the absence of He are computed. Next, a He atom is inserted at the desired location and the total forces F_{X+He} on X atoms in the presence of He are computed. Subtracting F_X from these forces gives F_{He-X}, the increment of force on any atom X due to the presence of He:

$$F_{He-X} = F_{X+He} - F_X. \tag{1}$$

This method is employed to calculate the forces on configurations of X atoms obtained during several steps of conjugate gradient energy minimization relaxation of He octahedral, tetrahedral and substitutional impurities in the metal lattice in DFT. In addition, forces acting on metal atoms by a He octahedral interstitial shifted to low symmetry locations along the $\langle 1\,0\,0\rangle$, $\langle 1\,1\,0\rangle$ and $\langle 1\,1\,1\rangle$ directions are also calculated using equation (1). Figure 1 illustrates this calculation on the example of a relaxed He octahedral interstitial in fcc Cu.

3. Results

He–Cu forces calculated by all three of the methods introduced above are presented in figure 2. Lattice expansion calculations are performed for a He octahedral interstitial in an 8-atom fcc Cu matrix using both GGA and LDA. In both cases, He only interacts with its nearest neighbor Cu

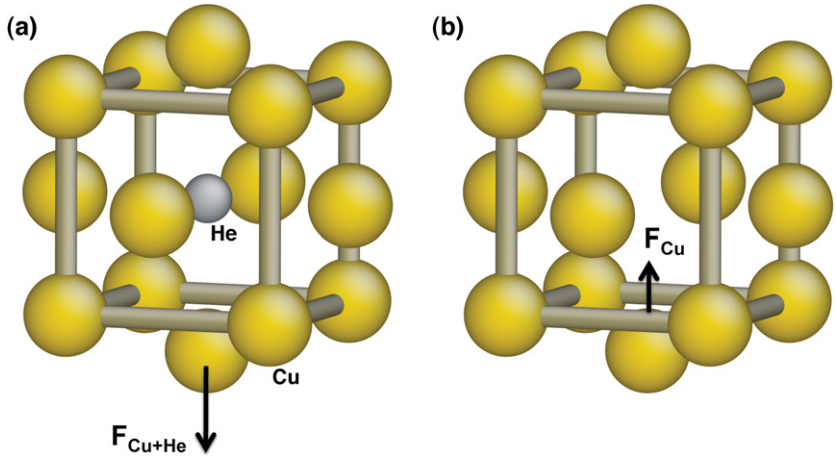

Figure 1. For a relaxed He octahedral interstitial (gray) in fcc Cu (yellow), He–Cu interatomic forces, $F_{He–Cu}$, are computed as differences between (*a*) the total force on Cu atoms in the presence of He, F_{Cu+He} and (*b*) forces exerted by Cu atoms on each other in the absence of He, F_{Cu} (see equation (1)).

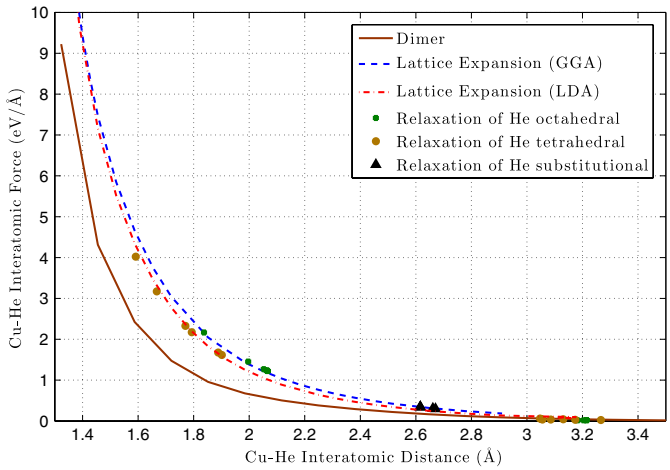

Figure 2. He–Cu force–distance curves, $F_{Cu–He}(r)$, calculated using the three different methods described in the text. The force–distance curve obtained from GGA lattice expansion calculation used to fit the Cu–He potential is in good agreement with force–distance data calculated from the relaxation of He defects in a 27-atom fcc Cu supercell.

atoms, no Cu atom interacts with more than one He atom and the He–Cu force–distance curves match closely, despite the different properties of pure Cu predicted by GGA and LDA (table 1). He–Cu forces determined from various stages in the relaxation of He octahedral, tetrahedral and substitutional impurities in a 27-atom fcc Cu crystal are in excellent agreement with the lattice expansion simulations, indicating that the forces do not depend on the detailed structure of He atom environments. The centrality of all He–Cu forces is confirmed by shifting a He octahedral interstitial to low symmetry locations along the ⟨1 0 0⟩, ⟨1 1 0⟩ and ⟨1 1 1⟩ directions and confirming that the angle between the Cu–He force and radius vectors is zero. This result may be explained directly from the electronic charge densities computed in DFT.

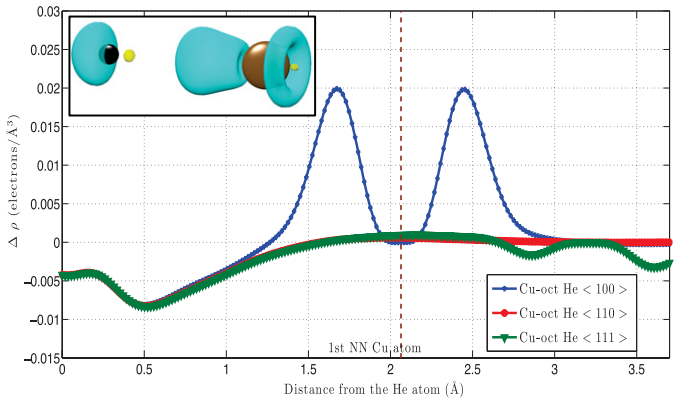

Figure 3. Plot of the redistribution of charge density, $\Delta\rho$, for an octahedral He interstitial in fcc Cu along the $\langle 1\,0\,0\rangle$, $\langle 1\,1\,0\rangle$, $\langle 1\,1\,1\rangle$ directions. The He atom is at the origin and the distance to the first nearest neighbor (NN) Cu atom is shown. The inset shows the ± 0.02 electron $\text{Å}^{-3}\,\Delta\rho$ isosurface for the Cu (right)-He (left) dimer. Positive charge density differences are in yellow and negative in blue.

The relaxed charge density distribution around the octahedral He defect in fcc Cu, $\rho_{\text{Cu+He}}$, is compared with the superposition $(\rho_{\text{Cu}} + \rho_{\text{He}})$ of the ground state charge densities of the same system without the He impurity ρ_{Cu} (i.e. containing Cu atoms only) and an isolated He atom ρ_{He}. The difference between $\rho_{\text{Cu+He}}$ and $(\rho_{\text{Cu}} + \rho_{\text{He}})$ gives $\Delta\rho$, the redistribution of the charge density in the electronic ground state of the combined system:

$$\Delta\rho = \rho_{\text{Cu+He}} - (\rho_{\text{Cu}} + \rho_{\text{He}}). \tag{2}$$

Values of $\Delta\rho$ as a function of distance from a He octahedral along three crystallographic directions are shown in figure 3.

In the case of the octahedral He interstitial in fcc Cu, the largest variation in charge density occurs along the $\langle 1\,0\,0\rangle$ direction between the Cu and He atom. Charge is depleted around the He atom and builds up around its first nearest neighbor. The energy associated with $\Delta\rho$ is estimated by taking the difference in the relaxation energies of the electronic charge densities of the combined Cu–He system and that of the same system without the He impurity (the self-consistent electronic charge density relaxations are initialized to a superposition of atomic orbital densities in both cases). This energy difference is on the order of 1.2 eV or 0.1 eV per Cu–He bond: a low value that can be attributed to the high first ionization energy and zero electron affinity arising from the closed shell electronic structure of He. The charge density distribution obtained by the superposition of the charge densities of fcc Cu and an isolated He atom is therefore a good approximation to the ground state charge density of He defects in Cu.

We use this insight along with the Hellmann–Feynman equation [25, 26] (equation (3)) to demonstrate the centrality of He–Cu forces:

$$F_{\text{Cu}} = -\int \rho(r)\frac{\partial v_{\text{Cu}}(r - R_{\text{Cu}})}{\partial R_{\text{Cu}}}\,\mathrm{d}r - \frac{\partial E_{\text{N}}(\{R\})}{\partial R_{\text{Cu}}} - \int \frac{\delta E_{\text{N}}(\{R\})}{\delta\rho(r)}\frac{\partial\rho(r)}{\partial R_{\text{Cu}}}\mathrm{d}r. \tag{3}$$

In the above expression, $\rho(r)$ is the electronic charge density for the spatial configuration of nuclei, $\{R\}$. The force on a Cu atom, F_{Cu}, with nuclear coordinates R_{Cu} arises from the electron–nucleus Coulombic interaction, $v_{\text{Cu}}(r - R_{\text{Cu}})$, and the nucleus–nucleus Coulombic interaction, $E_{\text{N}}(\{R\})$. According to the variational principle [27], the last term in equation (3) vanishes identically for the ground state charge density, which we assume to be the superposition of the charge densities of fcc Cu and an isolated He atom: $\rho = \rho_{\text{Cu}} + \rho_{\text{He}}$.

Substituting this expression into equation (3) and subtracting the forces exerted by the other Cu atoms in the absence of the He atom, we obtain an expression for the Cu–He force:

$$F_{\text{He–Cu}} = -\frac{Z_{\text{Cu}}}{4\pi\varepsilon_0}\int \frac{\rho_{\text{He}}(r)}{(r - R_{\text{Cu}})^2}\,\mathrm{d}r + \frac{Z_{\text{Cu}}Z_{\text{He}}}{4\pi\varepsilon_0(R_{\text{He}} - R_{\text{Cu}})^2}, \tag{4}$$

where ε_0 is the permittivity of vacuum, Z_{Cu}, Z_{He} are the atomic numbers and R_{Cu}, R_{He} are the nuclear coordinates of Cu and He, respectively. The second term on the right-hand side of equation (4) is the Cu–He nuclear interaction: a radially repulsive force. Because the charge density of an isolated He atom is spherically symmetric, the first term on the right-hand side of equation (4) yields a radially attractive force. Thus, equation (4) demonstrates that the Cu–He interatomic force is central if the ground state charge density is $\rho = \rho_{\text{Cu}} + \rho_{\text{He}}$.

Figure 2 shows that the force–distance curves obtained by different methods for He in fcc Cu are in excellent agreement, but the force–distance curve obtained form a Cu–He dimer calculation is markedly different. This too can be explained from an investigation of charge densities. The charge density redistribution $\Delta\rho$ was computed for the Cu–He dimer using equation (2). The energy decrease per Cu–He bond of 0.2 eV associated with $\Delta\rho$ for the dimer is larger than that in the case of the He octahedral in fcc Cu. The $\Delta\rho = \pm 0.02$ electrons Å^{-3} isosurface is shown as an inset in figure 3. The largest magnitude of $\Delta\rho$ occurs along the dimer axis and is twice that for He defects in fcc Cu. In contrast to He in fcc Cu, the charge density redistribution along the dimer axis increases near the He atom. Therefore, the ground state charge density of a Cu–He dimer is a poor approximation to the ground state charge density of He defects in fcc Cu.

A similar procedure to the one described above is employed to obtain the Nb–He force as a function of interatomic distance. 8 Nb atoms are used in lattice expansion simulations and 16 atoms in He interstitial and substitutional simulations. All forces are central, limited in range to Nb second nearest neighbors, and collapse onto a single force–distance curve. He–He interactions are studied by inserting He dimers and trimers into octahedral sites in fcc Cu and bcc Nb. Distances between He atoms are varied by systematically changing the position of any 1 He atom while keeping the positions of all other atoms fixed, thereby allowing the He–He force–distance curve to be computed. The He–He force–distance curve obtained from DFT predicts an equation of state for He in good agreement with experiment [28]. As in the case of He–Cu and He–Nb, He–He forces are found to be central and limited to nearest neighbors.

The force–distance curves obtained from the lattice expansion calculations are integrated to obtain two-body He–Cu, He–Nb and He–He interaction energies $V(r)$ [29]. Following Derlet *et al* [30], these can be expressed as a sum of cubic knot functions,

$$V(r) = \sum_{n=1}^{N} V_n(r_n - r)^3\Theta(r_n - r), \tag{5}$$

where $\Theta(x)$ is a Heaviside step function defined as ($\Theta(x) = 1$ for $x > 1$ and $\Theta(x) = 0$ for $x < 0$). The parameters V_n and r_n are optimized to reproduce the $V(r)$ computed from DFT. The complete parameterization of the three interatomic potentials is presented in table 2.

The two-body energies in table 2 may be combined with any Cu or Nb potentials to model Cu–He and Nb–He systems. We joined them with an existing embedded atom method (EAM) Cu–Nb potential [31]. Energies of He octahedral, tetrahedral and substitutional impurities in 27-atom fcc Cu supercells and 16-atom bcc Nb supercells calculated with the resulting Cu–Nb–He potential are in excellent agreement with values obtained from DFT, as shown in table 3. In computing these values, we define the He defect formation energy, $E^{\text{f}}_{\text{defect}}$, as

$$E^{\text{f}}_{\text{defect}} = E^{\text{final}}(nX, 1\text{He}) - E^{\text{initial}}(nX) - 1E_{\text{He}}, \tag{6}$$

Table 2. Parameters describing He–Cu, He–Nb and He–He two-body energies, $V(r)$.

Cu–He		Nb–He		He–He	
r_n (Å)	V_n (eV Å^{-3})	r_n (Å)	V_n (eV Å^{-3})	r_n (Å)	V_n (eV Å^{-3})
0.404 8597	264.830 3863	0.457 0914	142.011 2005	0.258 5328	2559.386 7828
0.729 9170	266.921 9661	0.827 320 78	143.119 6654	0.461 8739	2271.411 5660
1.055 9855	266.702 3756	1.198 9221	143.525 7463	1.105 5558	25.437 2712
1.362 8823	154.078 0438	1.546 0834	86.921 1775	1.499 6950	6444.414 0158
1.954 9572	7.616 6009	2.140 4260	6.126 6237	1.500 0000	6428.869 0273
3.461 7013	0.189 0666	3.822 2607	0.121 8639	2.006 232	2.633 8297

Table 3. Calculated defect energies for He substitutional, tetrahedral and octahedral defects in Cu and Nb.

	Cu			Nb		
	DFT (eV)	EAM (eV)	EAM (converged) (eV)	DFT (eV)	EAM (eV)	EAM (converged) (eV)
Octahedral	4.0325	4.0612	4.004	3.7147	3.7500	3.5666
Tetrahedral	4.1627	4.2372	4.1450	3.4547	3.7073	3.4515
Substitutional	1.4281	1.6494	1.5617	1.4158	0.8792	0.8131

where n is the number of metal atoms of type X, $E^{\text{final}}(nX, 1\text{He})$ is the energy of the relaxed defect configuration, $E^{\text{initial}}(nX)$ is the energy of the n metal atoms in the initial configuration without He and E_{He} is the energy of an isolated He atom. We assumed an ideal gas reference bath for He, where its chemical potential is 0 eV. The agreement between defect energies computed by DFT and our potential shown in table 3 are in excellent agreement, despite the fact that the potential was not fitted to these energies.

The small discrepancies in He defect energies found by DFT and our potential are due primarily to differences in the calculated properties of Cu and Nb, which may be influenced by the structure of local atomic environments. We attempted to determine whether these discrepancies are best correlated with the coordination of the defect site, its background charge density, or three-body interactions among Cu and Nb atoms neighboring the defect site. As Seletskaia [32], we find that three-body interactions best describe the discrepancies, but do not incorporate them into our potential since the error introduced by omitting them is small and does not justify the additional complexity involved.

The validity of the potential is further tested by comparing the energies and forces computed in DFT and using the potential in a 27-atom fcc Cu system with the He atom inserted mid-way between the center of an octahedral site and the nearest neighbor Cu atom. The force acting on the nearest Cu atom predicted by the potential is 114.8 eV Å^{-1}, which agrees well with DFT prediction of 114.6 eV Å^{-1}. The energy of the system calculated by the potential 24.57 eV is also in good agreement with the DFT value of 23.75 eV.

Since He interactions with Cu and Nb are short range and radial, a He impurity atom may be viewed as a soft misfitting sphere around which Cu and Nb atoms relax elastically. Therefore, any dependence of He defect energies on system size most likely arises from overlap of the elastic fields of periodic images of the defect. To validate this claim, we calculate the formation energy of an octahedral He defect in a 64-atom fcc Cu supercell using the constructed EAM potential and DFT. The potential gives 4.0296 eV, in good agreement with the DFT value of 4.003 eV. The decrease in octahedral defect energy due to increase in system size from 27 to 64 atoms is 0.0295 eV as predicted by DFT, while the decrease predicted by the

EAM potential is 0.0316. We use our potential to study the convergence of He octahedral, tetrahedral and substitutional energies with system size in both Cu and Nb. Converged He defect energies are obtained using a 4000 atom fcc Cu supercell and a 6750 atom bcc Nb supercell and are given in table 3. In all cases, the energy of the He defect decreases with increasing system size. However, the relative stability of defects in both fcc Cu and bcc Nb is not altered.

Our potential may be considered predictive since it is able to compute accurate defect formation energies despite not being fitted to them. Furthermore, we expect that it is transferrable to other structures containing He in condensed phases of Cu or Nb on the grounds of our understanding of the effect of He impurities on total electronic charge density.

4. Conclusions

We have constructed a repulsive Cu–Nb–He pair potential and shown that it is sufficient to describe He interactions in condensed Cu and Nb. The He defect formation energies predicted by the potential are in good agreement with DFT data. This work provides an example of constructing a predictive and transferable empirical potential based directly on the underlying interatomic bonding physics.

Acknowledgments

This work was funded by the LANL Directed Research and Development (LDRD) program. Discussions with Kedarnath Kolluri, Nicolas Poilvert, Mukul Kabir, Jiahao Chen and Richard E Baumer are gratefully acknowledged.

References

[1] Stoller R E 1990 *J. Nucl. Mater.* **174** 289
[2] Trinkaus H and Singh B N 2003 *J. Nucl. Mater.* **323** 229
[3] Stoller R E and Odette G R 1988 *J. Nucl. Mater.* **154** 286
[4] Lucas A A 1984 *Physica* B **127** 225
[5] Singh B N and Foreman A J E 1981 *J. Nucl. Mater.* **103–104** 1469
[6] Ullmaier H and Trinkaus H 1992 *Mater. Sci. Forum* **97–99** 451
[7] Hochbauer T, Misra A, Hattar K and Hoagland R G 2005 *J. Appl. Phys.* **98** 123516
[8] Misra A, Demkowicz M J, Zhang X and Hoagland R G 2007 *JOM* **59** 62
[9] Demkowicz M J, Bhattacharyya D, Usov I M, Wang Y Q, Nastasi M and Misra A 2010 The effect of excess atomic volume on He bubble formation at fcc-bcc interfaces *Appl. Phys. Lett.* **97** 161903
[10] Wilson W D and Bisson C L 1971 *Phys. Rev.* B **3** 3984
[11] Kobayashi N 1984 *J. Phys. Soc. Japan* **53** 3018
[12] Wedepohl P T 1967 *Proc. Phys. Soc.* **92** 79
[13] Giannozzi P *et al* 2009 *J. Phys.: Condens. Matter* **21** 395502
[14] Rappe A M, Rabe K M, Kaxiras E and Joannopoulos J 1990 *Phys. Rev.* B **41** 1227
[15] Vanderbilt D 1990 *Phys. Rev.* B **41** 7892
[16] Perdew J P, Burke K and Ernzerhof M 1996 *Phys. Rev. Lett.* **77** 3865
[17] Perdew J P and Zunger A 1981 *Phys. Rev.* B **23** 5048
[18] Fuchs M, Bockstedte M, Pehlke E and Scheffler M 1998 *Phys. Rev.* B **57** 2134
[19] Favot F, Dal Corso A and Baldereschi A 2001 *J. Chem. Phys.* **114** 483
[20] Ashcroft N W and Mermin D N 1976 *Solid State Physics* (New York: Holt)
[21] Smithells C J, Brandes E A and Brook G B 1992 *Metals Reference Book: Smithells Metals Reference Book* (London: Butterworth-Heinemann)
[22] Simmons G and Wang H 1971 *Single Crystal Elastic Constants and calculated aggregate properties: a handbook* (Cambridge, MA: MIT Press)
[23] Gray D E 1972 *American Institute of Physics Handbook* (New York: McGraw-Hill)

[24] Kittel C 1986 *Introduction to Solid State Physics* (New York: Wiley)
[25] Hellmann H 1937 *Einführung in die Quantenchemie* (Leipzig: Franz Deuticke)
[26] Feynman R P 1939 *Phys. Rev.* **56** 340
[27] Hohenberg P and Kohn W 1964 *Phys. Rev.* **136** B864
[28] Mills K, Liebenberg D H and Bronson J C 1980 *Phys. Rev.* B **21** 5137
[29] Ercolessi F and Adams J B 1994 *Europhys. Lett.* **26** 583
[30] Derlet P M, Nguyen-Manh D and Dudarev S 2007 *Phys. Rev.* B **76** 054107
[31] Demkowicz M J and Hoagland R G 2009 *Int. J. Appl. Mech.* **1** 421
[32] Seletskaia T, Osetskiy Yu N, Stoller R E and Stocks G M 2007 *J. Nucl. Mater.* **367–370** 355